Scripta Materialia 114 (2016) 51–55

Contents lists available at ScienceDirect

Scripta Materialia

journal homepage: www.elsevier.com/locate/scriptamat

The role of back stress in sub-50 nm Si nanocubes

E.D. Hintsala *[,1], A.J. Wagner [1], W.W. Gerberich, K.A. Mkhoyan **

Department of Chemical Engineering and Materials Science, University of Minnesota, United States

ARTICLE INFO

Article history:
Received 11 November 2015
Received in revised form 2 December 2015
Accepted 3 December 2015
Available online xxxx

Keywords:
Silicon
Nanoparticles
Work hardening
Back stress
Dislocations

ABSTRACT

Development of more accurate descriptions of dislocation motion requires understanding the actual effective stress driving it. Back stresses from dislocation pile-ups can work against the applied stress resulting in lower stresses acting on moving dislocations. This study presents calculations of back stress derived from in-situ compression of 26–39 nm sized single crystal silicon cubes inside the transmission electron microscope. These initially dislocation free particles exhibited yielding culminating in over 60% plastic strain. The back stress was calculated based on a pile-up model which, when subtracted from the applied stress, suggests a constant effective stress for continuing plasticity.

Dislocation pile-ups resulting in back stresses are important phenomena for understanding strengthening mechanisms, especially in nanoscale crystals. Nanoscale materials displaying near theoretical strengths have been observed for several years [1,2]. However, there has been no discrete analysis of the impact of back stresses on the flow stress, i.e. the applied stress necessary to maintain plastic deformation. High strength and toughness of nanomaterials [3,4] promises a bright future for nanotechnologies for a variety of applications but one which requires detailed understanding of how properties vary based upon different loading conditions, including strain rate effects and plastic confinement.

Garcia-Manyes and Guell [5] and Mook et al. [6] measured stresses at the indenter contact surface (i.e. contact stress) in nanoscale Si approaching and exceeding the theoretical strength, $E/10 = 16$ GPa [7]. The measured contact stress of 17 GPa for 1–12 nm depth indentations into silicon by a diamond indenter tip mounted to an atomic force microscope (AFM) [5] slightly exceeds the theoretical strength according to the E/10 determination. Compression of 40–140 nm diameter Si nanospheres [6] presented an even more compelling case as the measured contact stresses appear to exceed the theoretical strength even when dividing by the factor associated with a triaxial stress state. In both cases significant plastic deformation was nucleated and the contact stresses are comparable when scaled by the plastically deformed volume. This was approximated by relating the size of the plastically deformed Si spheres to the calculated plastic zone diameter $4a$, where a is the contact radius of the indented Si. This suggests that there exists a strong correlation between plastic zone size and contact stress. In both cases theoretical strength level stresses are maintained for plastic zone sizes up to about 60 nm. This originally was explained as a pressure effect [8]. However, previous studies have shown that the contact stress should drop as dislocations are nucleated, which was not observed in either case [9]. In both cases, substantial plasticity was present and, therefore, these high strengths cannot be explained by a pressure effect. It should be noted that differences may be due to the relative size of contact, the amount of confinement and the dislocation velocities or Peierls barriers in relation to effective stresses.

The presence of previously emitted dislocations exerting an elastic stress on the indenter due to their lattice distortion (a back stress) could explain these high strengths as the measured applied stress would not be the true effective stress for dislocation nucleation and motion. Nanoscale materials possess an inherent limitation on the number and separation of dislocations within their volume, producing large back stresses relative to the bulk [6,10,11]. Analysis of the discrete contribution of the back stress from dislocations is challenging due to the need for high precision mechanical measurements and imaging, as well as a dislocation-free specimen with a readily interpretable geometry. Some efforts have been made to analyze back stresses from conventional nanoindents, using etch pit decoration of dislocations for MgO [12] and using AFM for KBr [13]. These techniques can only detect surface dislocations, however, resulting in somewhat limited applicability. Here we present an experimental analysis of back stresses due to dislocation pile-ups during compression of single-crystal Si nanocubes (NCs), which can be considered as a nearly ideal experiment for studying dislocation-induced back stresses.

* Correspondence to: E.D. Hintsala, 454 Amundson Hall, 421 Washington Ave SE, Minneapolis, MN 55414, United States.
** Correspondence to: K.A. Mkhoyan, 34 Amundson Hall, 421 Washington Ave SE, Minneapolis, MN 55414, United States.
E-mail addresses: hints009@umn.edu (E.D. Hintsala), mkhoyan@umn.edu (K.A. Mkhoyan).
[1] These authors contributed equally to this work.

http://dx.doi.org/10.1016/j.scriptamat.2015.12.004
1359-6462/

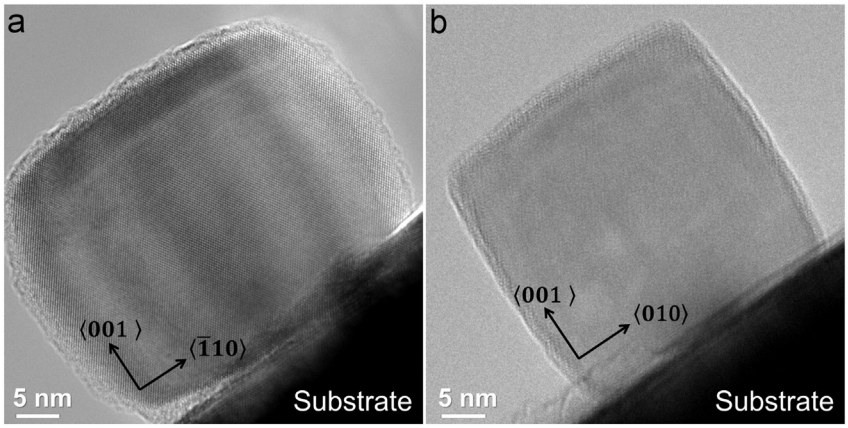

Fig. 1. TEM images of {100}-faceted Si NCs oriented such that its (a) [110] direction and (b) [100] direction is along the beam direction.

Si NCs 26 nm to 39 nm in size and terminated by <100> facets (Fig. 1), previously shown to be nominally defect free [14], were individually compressed along the [001] direction with a Hysitron PI-95 PicoIndenter. NCs were synthesized in a plasma reactor, as described earlier [15,16] and deposited directly onto small sapphire pieces with a sharp edge which allowed unobstructed transmission electron microscopy (TEM) imaging during compression. NCs were compressed using a nominally flat, boron-doped diamond tip with a strain rate of 0.1–0.2 s^{-1}. Compressions were performed in an FEI Tecnai F30 Scanning-TEM operating at 200 keV while acquiring zero-loss filtered conventional TEM images at 25 fps to produce videos using a Gatan 692 CCD camera.

True stress-true strain curves for compressed 26 to 39 nm NCs are shown in Fig. 2a. Full discussion of the mechanical data and investigation into the mechanisms of plasticity in these Si NCs is available in [17], but will be briefly reiterated here. First, linear elasticity is maintained up to about 7% true strain, called "regime i." A deviation from linearity occurs corresponding to formation of dislocation embryos ("regime ii") (possibly a local β-tin phase transformation) up to an upper yield point at 11% true strain and 11 GPa stress. At the upper yield point, dislocation activity on {111} planes is observed ("regime iii") as the stress begins to drop which could result from increased stress concentration due to the nucleated surface steps, decreased local volume associated with the phase transformation or rapid dislocation emergence at the free surfaces of the NCs. The same planes continue to flicker as the stress drops to a lower yield point at 40–50% true strain and 8 GPa true stress ("regime iv"). Following the lower yield point, linear hardening is observed to occur up to 70% strain ("regime v").

During the drop from the upper yield point to the lower yield point, it is believed that dislocations are freely terminating at the truncated corners of the NC. This interpretation is supported by repeated compression of a 45 nm Si NC whose stress–strain curves are seen in Fig. 2b. Initial compression of the NC was aborted at the first sign of yielding, and then was repeatedly compressed with displacements of approximately 5 nm. Between each compression the NC height and width were measured and used to offset each curve. The upper and lower yield stresses are comparable to continuous compressions. The mismatch between the unloading NC height at zero load and post-mortem measurement suggests that a significant amount of reverse plasticity, i.e. dislocations reversing their path back to the nucleation

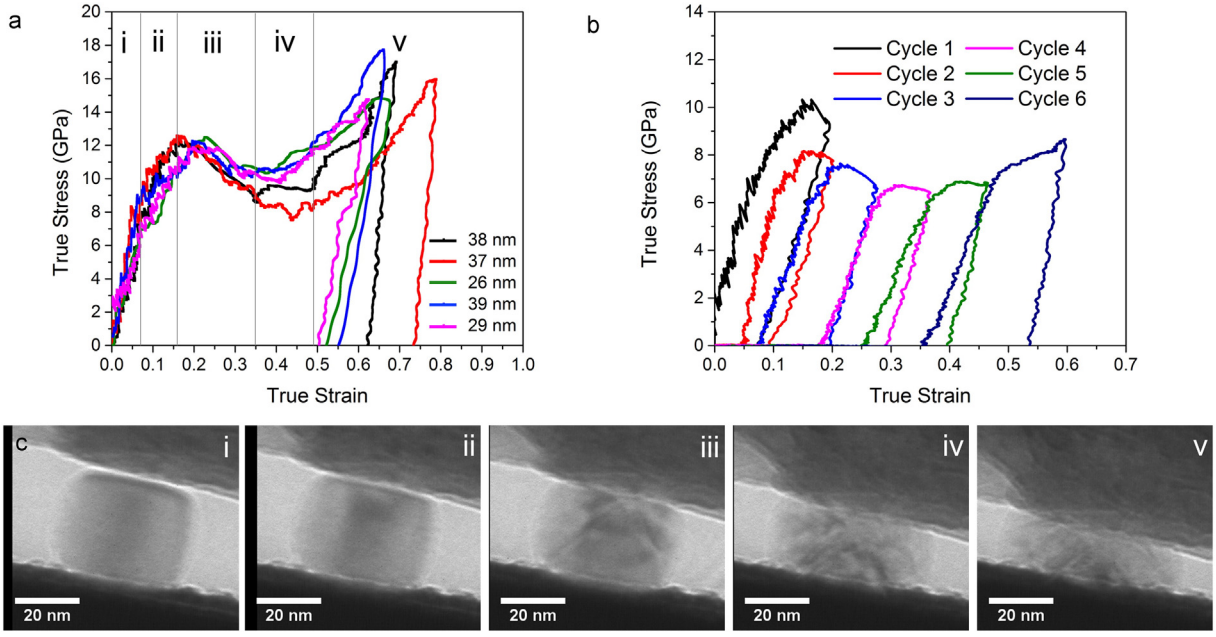

Fig. 2. (a) True stress vs. true strain curves for analyzed Si NCs, all showing identical deformation regimes (i–v) but with some variance in stress and strain levels for the onset of each. (b) True stress vs. true strain curves for repeat compression of a 45 nm Si NC obtained in displacement control mode. NC height was measured between compressions. The first compression was aborted upon observation of {111}-habit contrast. Subsequent compressions were terminated at a target displacement of 5 nm. (c) Images from in-situ TEM compression video, which are representative of each deformation regime (i–v) for the 38 nm particle.

surface [18], occurs on unloading. Observation of reverse plasticity means that the dislocations are not trapped and by extension that the NCs are nearly dislocation free at the start of each subsequent cycle until hardening begins.

Dislocation activity was observed to occur on the {111} slip planes. Dislocation emission starts at the center of the contact surface where a stress concentration exists with growth in the $[\bar{1}10]$ direction for dislocations as depicted in Fig. 2c (i–v). Back stresses develop in the linear hardening regime as the NC has been deformed to such degree that a fully flat contact is made between it and the indenter with the substrate trapping future emitted dislocations as illustrated in Fig. 3a. The onset of dislocation confinement would require approximately 33% plastic strain, based on the observation that the body and face diagonals were 1.25 times the NC height. This 33% plastic strain added to the observed 11% elastic strain matches the observed onset of linear hardening at about 45% strain.

In order to estimate the back stress exerted by dislocations nucleated during the linear hardening regime, we developed a model adapted for the specific geometry of these NCs. The Eshelby dislocation pile-up model [19] for back stress, τ_{BS}, is given by

$$\tau_{BS} = \frac{\mu b N_{eff}}{2\pi l_s(1-\nu)}. \tag{1}$$

Here, N_{eff} is an effective number of dislocations in a pile-up, μ and ν are the elastic constants, b is the Burgers vector and l_s is the distance from the leading dislocation of the pile-up to the source [19].

First, the shear stress needs to be resolved into normal stress acting on the indenter NC contact surface. The shear area needs to be determined, for which two limiting cases are considered as illustrated in Fig. 3b. Assuming the slip plane angle remains constant as deformation proceeds the shear area is a trapezoid (shown in red in Fig. 3b) which depends on the instantaneous height, h_i, and instantaneous width, w_i. However, some rotation of the slip planes is expected. In the limiting case where the slip plane angle varies to its maximum degree and the corners of the {111} plane remain fixed, the shear area is triangular (shown in blue in Fig. 3b). These two models for the shear area depend on w_i and h_i as:

$$A_S = \begin{cases} \left(\frac{\sqrt{3}}{2}\right) h_i(2w_i - h_i) & trapezoidal \\ \left(\frac{\sqrt{2}}{2}\right) w_i \sqrt{\frac{1}{2}w_i^2 + h_i^2} & triangular \end{cases} \tag{2}$$

The true shape of the slip planes would be somewhere between the limiting trapezoidal and triangular cases described. Multiplying the stress (Eq. (1)) by the shear area (Eq. (2)) gives the force along the slip direction. With the shear stress, τ_{BS}, equal to half of the normal compressive stress, σ_{BS}, for a uniaxial stress state and resolving the force $F_N = \sigma_{BS} w_i^2$ in the normal direction required to resist the compressive force one finds

$$\sigma_{BS} w_i^2 = 2\tau_{BS} A_S \cos\theta. \tag{3}$$

With $\cos\theta = 1/\sqrt{2}, l_s = \sqrt{3/2}h_i$ for the trapezoidal shear area or $l_s = \sqrt{1/2w_i^2 + h_i^2}$ for the triangular shear area, Eqs. (2) and (3) can be combined to give the back stress acting over the normal area of the cube face

$$\sigma_{BS} = \begin{cases} \frac{\mu b N_{eff}(2w_i - h_i)}{2\pi(1-\nu)w_i^2} & \text{trapezoidal} \\ \frac{\mu b N_{eff}}{2\pi(1-\nu)w_i} & \text{triangular} \end{cases} \tag{4}$$

N_{eff} will need to be estimated not being able to fully characterize the exact arrangement of dislocations or their number. Here, $N_{eff} \propto \varepsilon_p$ where ε_p is the confined plastic strain. The onset of the linear hardening regime, $\varepsilon_{0,LH,}$ is used as the beginning of confined plastic strain such that $\varepsilon_p = \varepsilon - \varepsilon_{0,LH}$ and it is estimated that $N_{eff} \approx \sqrt{2}\varepsilon_p h_0/b$, based on the change in particle height due to the emission of one dislocation.

This model does not explicitly depend on the dislocation character as the final solution is Burgers vector independent. The model is derived for trapped perfect edge dislocations for simplicity even though partial dislocations were observed in [17] just after the upper yield point, though the dislocation character in the hardening regime could not be characterized. This is a reasonable approximation as each pair of partial dislocations would produce a similar stress field to a perfect dislocation. However, it should be noted that the spacing between dislocations in the pile-up would likely be different. The effect of dislocation character would exist in the stress field of each individual dislocation through the $(1\text{-}\nu)$ factor, with a perfect screw dislocation requiring a change of $(1\text{-}\nu)$ to 1 resulting in the lowest possible stress field per dislocation.

A few other important approximations are: it is assumed that dislocations do not mutually annihilate or react to form Lomer locks [20] and dislocations do not escape in the hardening regime through other means such as climb. Additionally, it is assumed that the spacing between slip planes does not affect the back stress (which is observed in [21]). Lastly, the choice of μ and ν for a highly anisotropic material such as Si is not straightforward. The most simple assumption is to use $\mu = 67$ GPa and $\nu = 0.22$ which represents the isotropic averaged

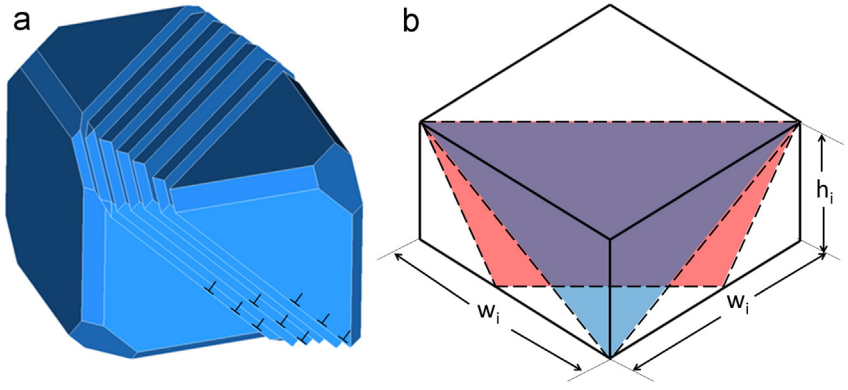

Fig. 3. (a) Illustration showing how a truncated NC achieves confined slip bands after plastic deformation. This only shows one set of slip bands for simplicity; a more realistic picture would use multiple slip bands to produce homogeneous deformation. (b) Illustration of trapezoidal (red) vs. triangular (blue) shear areas for a compressed cube, where the trapezoidal shear area maintains the original angle of the {111} plane and the triangular shear area allows maximum rotation. (For interpretation of the references to color in this figure legend, the reader is referred to the web version of this article.)

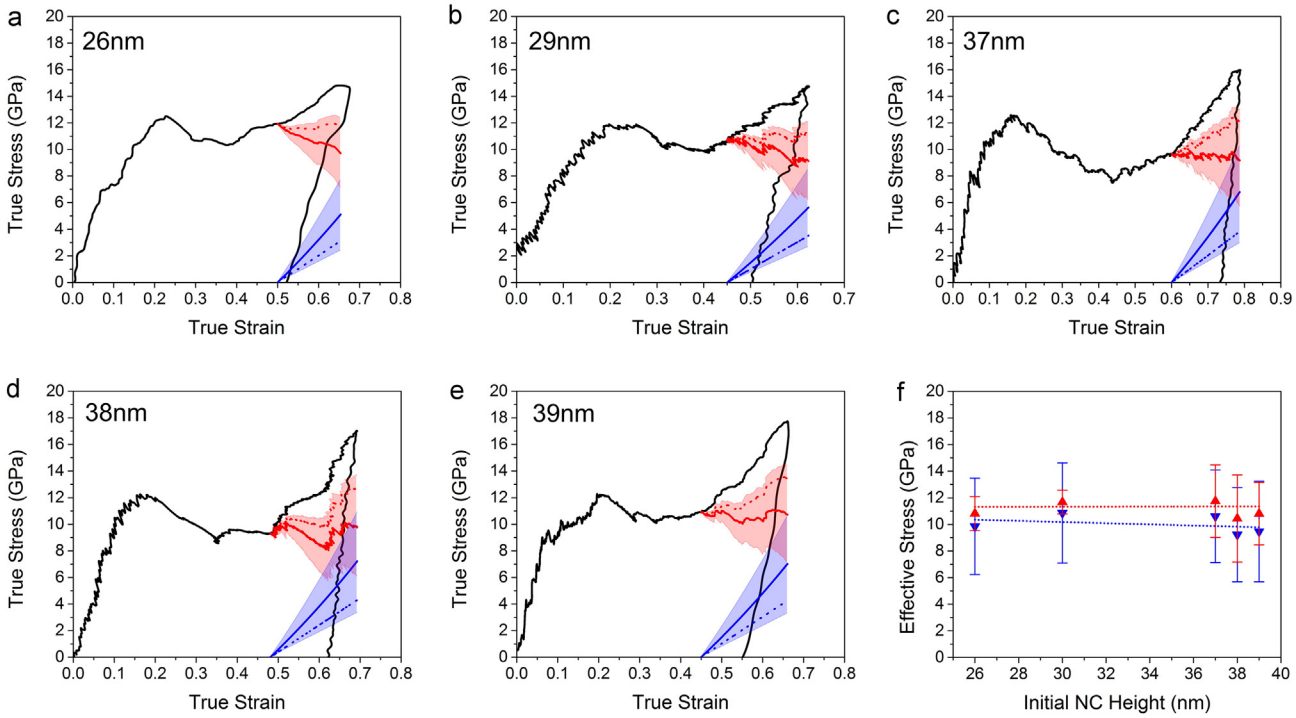

Fig. 4. (a–e) The calculated back stress (blue) and resulting effective stress (red) for particles of different sizes. Shading represents the range of possible values based on the selection of μ and ν. Dotted lines represent the triangular shear plane model and solid lines represent the trapezoidal shear plane model with $\mu = 67$ GPa and $\nu = 0.22$. (f) Effective stress is shown vs. NC size for the triangular and the trapezoidal models. Error bars represent the variation of μ and ν. The linear fit to the data is presented with a dotted line. (For interpretation of the references to color in this figure legend, the reader is referred to the web version of this article.)

values, but directional values could also be utilized, such as values on the {111} plane in <110> directions of $\mu = 62.4$ GPa and $\nu = 0.22$ [22].

It is clear from the in-situ TEM imaging that severely constrained plastic flow builds up large back stresses that contribute to the total flow stress. For a constrained volume, the effective stress can be evaluated as

$$\sigma_{eff} = \sigma_{flow} - \sigma_{BS}. \quad (5)$$

As has been discussed for decades, it is the effective stress that should be applied in the dislocation velocity expression as reduced by a back stress [19,23–30]. In constrained volumes the continued motion of dislocations is limited by the size of the NC and plasticity is controlled by additional dislocation nucleation at a constant effective stress.

Fig. 4 shows the compressive applied stress determined from contact areas measured from in-situ TEM videos, the back stress calculated from Eq. (4) and the difference that is the effective stress as indicated in Eq. (5). Calculations are performed for both trapezoidal and triangular shear area models. Additionally, shading for each model is utilized to demonstrate the maximum changes due to variation of μ from 58 GPa to 80 GPa and variation of ν from 0 to 0.28 to account for dislocation character changes. The onset of linear hardening tended to occur at stress levels very near the observed upper yield stress, resulting in the average effective stress for all the analyzed NCs to be 10.2 GPa. For these sub-50 nm volumes under compression it appears then that it may not be the initial yield strength that is length scale dependent but rather the flow stress which is back stress dependent in constrained flow. Additionally, it can be argued that it is the effective stress that is required for nucleating the next dislocation rather than the applied stress, which applies equally to calculations of dislocation velocity using a stress-dependent activation energy. This would imply that the dislocation velocity controls the strain rate sensitivity [29] and, in the present case, velocity is controlled through the effective stress. Such data will become necessary for validation of atomistic simulations as the temporal and temperature refinements become a reality [30–33].

A similar back stress analysis should be applicable to materials with other crystal structures and slip systems, assuming dislocation motion is the dominant plasticity mechanism and can be properly characterized. It should also be possible to account for other environmental variables affecting dislocation nucleation and propagation, such as temperature or impurities. In addition, pre-existing dislocations could be accounted for, especially if dislocation starvation [2] were to ensue prior to larger scale yielding. However, even initially trapped dislocations may not be problematic with appropriate modification of the methods utilized here, as guided by in-situ imaging. Stress gradients could be considered as well using finite element analysis. For this work, this would improve the calculation of dislocation pile-up spacing as there is a gradient due to barreling from contact friction. Such considerations would be critical for a more complex particle shape.

Acknowledgments

This work was supported in part by NSF MRSEC under awards DMR-0819885 and DMR-1420013. STEM analysis was carried out in the Characterization Facility of the University of Minnesota, which receives partial support from the NSF through the MRSEC program. The authors would like to thank Doug Stauffer and Ryan Major of Hysitron for their continued support.

References

[1] J. Wang, F. Sansoz, J. Huang, Y. Liu, S. Sun, Z. Zhang, S.X. Mao, Nat. Commun. 4 (2013) 1742.
[2] J.R. Greer, W.D. Nix, Phys. Rev. B 73 (2006) 245410.
[3] P.R. Howie, S. Korte, W.J. Clegg, J. Mater. Res. 27 (2012) 141–151.
[4] F. Östlund, K. Rzepiejewska-Malyska, K. Leifer, L.M. Hale, Y. Tang, R. Ballarini, W.W. Gerberich, J. Michler, Adv. Funct. Mater. 19 (2009) 2439–2444.
[5] S. Garcia-Manyes, A.G. Guell, P. Gorostiza, F. Sanz, J. Chem. Phys. 123 (2005) 114711/1–114711/7.
[6] W.M. Mook, J.D. Nowak, C.R. Perrey, C.B. Carter, R. Mukherjee, S.L. Girshick, P. McMurry, W.W. Gerberich, Phys. Rev. B 75 (2007) 214112–211/10.
[7] J. Frenkel, Z. Phys. 37 (1926) 572–609.
[8] F.D. Murnaghan, Proc. Natl. Acad. Sci. U. S. A. 30 (1944) 244–247.

[9] C. Begau, A. Hartmaier, E.P. George, G.M. Pharr, Acta Mater. 59 (2011) 934–942.
[10] K.M. Youssef, R.O. Scattergood, K.L. Murty, J.A. Horton, C.C. Koch, Appl. Phys. Lett. 87 (2005) 091904.
[11] S.M. Han, T. Bozorg-Grayeli, J.R. Groves, W.D. Nix, Scr. Mater. 63 (2010) 1153–1156.
[12] P. Egberts, R. Gralla, R. Bennewitz, Phys. Rev. B 86 (2012) 035446.
[13] Y. Gaillard, C. Tromas, J. Woirgard, Acta Mater. 54 (2006) 1409–1417.
[14] M.J. Cordill, M.D. Chambers, M.S. Lund, D.M. Hallman, C.R. Perrey, C.B. Carter, A. Bapat, U. Kortshagen, W.W. Gerberich, Acta Mater. 54 (2006) 4515–4523.
[15] A. Bapat, M. Gatti, Y.P. Ding, S.A. Campbell, U. Kortshagen, J. Phys. D. Appl. Phys. 40 (2007) 2247.
[16] A.J. Wagner, C.M. Anderson, J.N. Trask, L. Cui, A. Chov, K.A. Mkhoyan, U.R. Kortshagen, Nano Lett. 13 (2013) 5735–5739.
[17] A.J. Wagner, E.D. Hintsala, P. Kumar, W.W. Gerberich, K.A. Mkhoyan, Acta Mater. 100 (2015) 256–265.
[18] W.W. Gerberich, W.M. Mook, M.J. Cordill, C.B. Carter, C.R. Perrey, J.V. Heberlein, S.L. Girshick, Int. J. Plast. 21 (2005) 2391–2405.
[19] J.D. Eshelby, F.C. Frank, F.R.N. Nabarro, Philos. Mag. 42 (1951) 351.
[20] A. Bourret, J. Desseaux, A. Renault, Philos. Mag. A 45 (1982) 1–20.
[21] J.Y. Shu, N.A. Fleck, E. van der Giessen, A. Needleman, J. Mech. Phys. Solids 49 (2001) 1361–1395.
[22] J. Kim, D. Cho, R.S. Muller, Proc. Transducers, 2001 662–665.
[23] J.D. Nowak, A.R. Beaber, O. Ugurlu, S.L. Girshick, W.W. Gerberich, Scr. Mater. 62 (2010) 819–822.
[24] M. Brede, P. Haasen, Acta Metall. 36 (1988) 2003–2018.
[25] T.E. Mitchell, P. Peralta, J.P. Hirth, Acta Mater. 47 (1999) 3687–3694.
[26] K. van Vliet, J. Li, T. Zhu, S. Yip, S. Suresh, Phys. Rev. B 67 (2003) 104105/1–104105/15.
[27] L. Pizzagalli, P. Beauchamp, Philos. Mag. Lett. 88 (2008) 421–427.
[28] J.L. Demenet, J. Rabier, X. Milhet, M.H. Hong, P. Pirouz, I. Stretton, P. Cordier, J. Phys. Condens. Matter 14 (2002) 12961.
[29] P.B. Hirsch, S.G. Roberts, Philos. Mag. A 64 (1991) 55–80.
[30] C.J. Healy, G.J. Ackland, MRS Proc. 1369 (2012).
[31] L.M. Hale, X.W. Zhou, J.A. Zimmerman, N.R. Moody, R. Ballarini, W.W. Gerberich, J. Appl. Phys. 106 (2009) 1–7.
[32] M.I. Mendelev, S. Han, D.G. Srolovitz, G.J. Ackland, D.Y. Sun, M. Asta, Philos. Mag. 83 (2003) 3977–3994.
[33] J.R. Kermode, T. Albaret, D. Sherman, N. Bernstein, P. Gumbsch, M.C. Payne, G. Csányi, A. de Vita, Nature 455 (2008) 1224–1227.